PAPER • OPEN ACCESS

Structural and optical properties of (1122) InGaN quantum wells compared to (0001) and (1120)

View the article online for updates and enhancements.

Related content

Structural and optical properties of (11$\bar{2}$2) InGaN quantum wells compared to (0001) and (11$\bar{2}$0)

Markus Pristovsek[1], **Yisong Han**[1,4], **Tongtong Zhu**[1], **Fabrice Oehler**[1,5], **Fengzai Tang**[1], **Rachel A Oliver**[1], **Colin J Humphreys**[1], **Darius Tytko**[2], **Pyuck-Pa Choi**[2], **Dierk Raabe**[2], **Frank Brunner**[3] and **Markus Weyers**[3]

[1] Department of Materials Science and Metallurgy, University of Cambridge, 27 Charles Babbage Road, Cambridge, CB3 0FS, UK
[2] Max-Planck-Institut für Eisenforschung GmbH, Department of Microstructure Physics and Alloy Design, Max-Planck-Straße 1, D-40237 Düsseldorf, Germany
[3] Ferdinand-Braun-Institut, Leibniz-Institut für Höchstfrequenztechnik, Gustav-Kirchhoff-Str. 4, D-12489 Berlin, Germany

E-mail: mp680@cam.ac.uk

CrossMark

Abstract

We benchmarked growth, microstructure and photo luminescence (PL) of (11$\bar{2}$2) InGaN quantum wells (QWs) against (0001) and (11$\bar{2}$0). In incorporation, growth rate and the critical thickness of (11$\bar{2}$2) QWs are slightly lower than (0001) QWs, while the In incorporation on (11$\bar{2}$0) is reduced by a factor of three. A small step-bunching causes slight fluctuations of the emission wavelength. Transmission electron microscopy as well as atom probe tomography (APT) found very flat interfaces with little In segregation even for 20% In content. APT frequency distribution analysis revealed some deviation from a random InGaN alloy, but not as severe as for (11$\bar{2}$0). The slight deviation of (11$\bar{2}$2) QWs from an ideal random alloy did not broaden the 300 K PL, the line widths were similar for (11$\bar{2}$2) and (0001) while (11$\bar{2}$0) QWs were broader. Despite the high structural quality and narrow PL, the integrated PL signal at 300 K was about 4× lower on (11$\bar{2}$2) and more than 10× lower on (11$\bar{2}$0).

(Some figures may appear in colour only in the online journal)

1. Introduction

Many efforts are currently under way to improve the efficiency of InGaN based light emitting diodes and lasers for long wavelengths. One approach uses semi- and non-polar orientations, which dramatically reduce the effect of the built-in polarisation and piezo-electric fields [1]. These fields are most pronounced in the polar (0001) orientation and lead to a reduced wave function overlap and a power dependent wavelength shift of the photo luminescence (PL) emission. An especially promising orientation is (11$\bar{2}$2), because it is a stable facet occurring spontaneously [2]. This allows for the

[4] Current address: Nanotechnology & Integrated Bio-Engineering Centre, University of Ulster at Jordanstown, Newtownabbey, BT37 0QB, UK.
[5] Current address: Laboratory for Photonics and Nanostructures, CNRS, Route de Nozay, 91460 Marcoussis, France.

use of patterned *r*-plane sapphire to realise low defect density templates suitable for industrial production [3–8]. Compared to template growth and devices, relative little work has been reported on the actual quantum wells (QWs). For instance, there have been contradicting reports in the literature on the indium incorporation into ($11\bar{2}2$) QWs. Some studies found In incorporation close to that on (0001) [9, 10] while others found the opposite [2, 11, 12]. However, the In content was often estimated from the PL peak wavelength. But the polarisation fields strongly change with surface orientation, the PL wavelengths can be quite different for a similar In content.

Since the ($11\bar{2}2$) orientation is titled by $58.4°$ from (0001) towards the ($11\bar{2}0$) orientation, the QWs were benchmarked against these two orientations. Recent reports using atom probe tomography (APT) found In clustering on the nanoscale on ($11\bar{2}0$) [13, 14] but not on (0001) [13, 15, 16]. An earlier work was consistent with semi-polar ($10\bar{1}\bar{1}$) InGaN QWs as a random alloys [17]. But ($11\bar{2}2$) QWs have never been investigated in APT so far.

Therefore, we optimised growth and studied microstructure and photoluminescence (PL) of InGaN QWs on semi-polar ($11\bar{2}2$) GaN and systematically benchmarked them against polar (0001) QWs and non-polar ($11\bar{2}0$) QWs.

2. Experimental

Our (0001) GaN templates on *c*-plane sapphire had typical dislocation densities of $2 - 4 \times 10^8 \, \text{cm}^{-2}$ and (0002) x-ray diffraction (XRD) full width at half maximum (FWHM) of 150–200″. The semi-polar templates were prepared at the Ferdinand-Braun-Institute on 100 mm patternd *r*-plane sapphire wafers [8], which were cut into $2 \, \text{cm}^2$ squares. From low temperature cathodoluminescence (CL) we found dislocation densities between 2×10^7 and $2 \times 10^8 \, \text{cm}^{-2}$, less than $500 \, \text{cm}^{-1}$ basal stacking faults (BSFs), and the symmetric ($11\bar{2}2$) XRD FWHM were around 250″ [8]. For comparison we used also a few ($11\bar{2}2$) templates produced by ammonothermal growth. We will refer to these templates as low defect densities templates (LDD) to differentiate them from semi-polar templates grown directly on *m*-plane sapphire which have higher dislocation densities (HDD) closer to 10^{10}cm^{-2} and more than $10^5 \, \text{cm}^{-1}$ stacking faults [18].

For ($11\bar{2}0$) we used either ammonothermal bulk substrates or hydride vapour phase epitaxy grown and cut quasi-bulk substrates (LDD), and on unpatterned *r*-plane sapphire (HDD) [19].

We stacked five InGaN QWs for investigating optical properties, but used also thicker InGaN layers for incorporation and critical thickness studies. The QW were grown in an Aixtron $6 \times 2″$ close-coupled showerhead reactor. The temperatures given in the paper are from emissivity corrected pyrometry using an EpiTT 3 wavelength system. First layer was a GaN buffer which was optimised for smooth semi-/ non-polar regrowth, i.e. at 5 kPa $11.5 \, \text{l min}^{-1}$ H$_2$ at $1060 \, °\text{C}$ with $8.5 \, \text{l min}^{-1}$ NH$_3$ and a V/III ratio of ≈ 1000, resulting in a growth rate of $\approx 5 \, \mu\text{m h}^{-1}$. Next were the optimised semi-

polar QWs (with respect to their PL intensity in the cyan range) the nitrogen flow was 11.4 slm N$_2$ at 40 kPa with HN$_3$ 10 slm, and the partial pressures were 0.06 Pa of TMIn, and 0.033 Pa of TEGa (a gas phase ratio of 64% In). The QW growth rate was $\approx 1.8 \, \text{nm min}^{-1}$. The QWs were then overgrown by 1.8 nm of GaN with the same growth rate as for the QWs. Afterwards the temperature was increased by $100 \, °\text{C}$ (setpoint) followed by a $5\times$ increased TEGa flow for the rest of the barrier. This is the so-called quasi two temperature (Q2T) barrier growth.

There are other barrier growth strategies. The simplest one is the growth at the same temperature for QWs and barriers. This results in the longest emission wavelength, but is prone to form trench defects on (0001) [20]. Therefore, we preferred the above Q2T growth, which results in well-defined QWs with reduced trench defect densities on (0001) [21–23] and ($1\bar{1}00$) orientations [24]. However, Q2T grown barriers have been reported on (0001) to show less QW PL intensity compared to the two temperature (2T) barrier growth, i.e. increasing the temperature directly after the QW [21]. But 2T growth yields more discontinuous QWs on (0001), where In content and QW thickness fluctuate strongly along the QWs [21]. Moreover, on ($11\bar{2}2$) the Q2T growth gave the highest intensity for a given wavelength and very well-defined QWs (as discussed later). Therefore, we used Q2T growth for all QWs in this study, even though we may have preferred 2T growth for (0001) QW.

The thickness of ($11\bar{2}2$) QWs and their microstructure were examined by transmission electron microscopy (TEM). [$1\bar{1}00$] zone cross-sectional thin foils were prepared by conventional mechanical polishing followed by Ar ion beam thinning. Diffraction contrast imaging and annular dark-field imaging were performed in an FEI Tecnai Osiris microscope operated at 200 kV.

Two ($11\bar{2}2$) QWs were measured by APT, employing a LEAP 3000X HR system (Cameca Instruments) in laser assisted mode at 100 kHz laser pulse frequency. The laser energy and detection rate were set to 0.05 nJ and 3%, respectively. The specimen base temperature during the measurement was set to $\approx 60 \, \text{K}$. The data were then reconstructed and analysed as previously reported [13, 25].

The In content and QW and barrier thickness for (0001) samples were obtained from XRD measurements of the symmetric (0002) reflection and dynamic simulation using the Epitaxy software package. The barrier growth rate was independently confirmed by *in situ* reflectance oscillation during growth of a thick layer at barrier growth conditions. For the ($11\bar{2}2$) orientation we recorded symmetrical $\omega - 2\Theta$ scans of the ($11\bar{2}2$) reflection along [$11\bar{2}3$] and [$1\bar{1}00$] and then did simulation using our own software [26, 27]. APT and TEM confirmed the XRD simulation results within the errors of $\approx 1\%$ for the In content. All of the QWs included in the study were fully strained, unless the one used to determine the critical thickness.

Room temperature (RT) PL was measured with an Accent RPM2000 PLM mapper, which uses a pulsed 266 nm laser with four attenuation settings (none, 1/3.9, 1/8.9, and 1/13.9) with an average power of $\approx 2.2 \, \text{mW}$ on the sample.
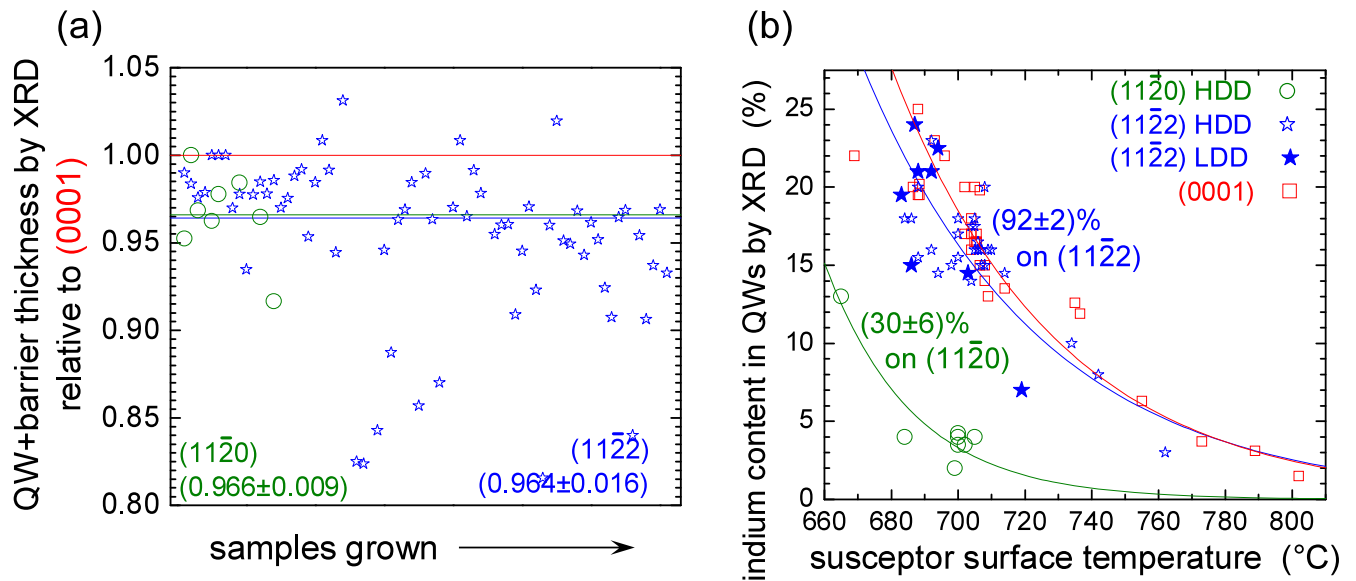
Figure 1. Relative change of growth rate (a) and dependence of In content from growth temperature (b) for various samples of simultaneous grown □ (0001), ⋆ (11$\bar{2}$2), and ○ (11$\bar{2}$0) QWs as obtained from x-ray diffraction. Due to the low intensity of the symmetric (11$\bar{2}$2) reflection, In contents below 5% were only accessible for thick (11$\bar{2}$2) InGaN layers, not for QWs.

We estimated from the saturation of the screening on (0001) that 2.2 mW excitation generates mid. 10^{19} cm^{-3} carriers inside each of five 3 nm (0001) 17% InGaN QW. We integrated the area under the peak.

3. Results

3.1. Growth

The (11$\bar{2}$2) has the same surface normal as a surface made out of (0001) and (11-20) facets which are each the same number of a_0 and c_0-lattice constants wide. Thus micro-faceting may occur during QW growth, like it has been observed e.g. on (20$\bar{2}$1) [28]. Therefore, we compared the (11$\bar{2}$2) to these two orientations.

Figure 1 compares growth rate and In incorporation of simultaneously grown QWs on (11$\bar{2}$0), (11$\bar{2}$2), and (0001). The growth rate in figure 1(a) is very similar for all orientations, on (11$\bar{2}$0) it is (96.6 ± 0.9)% and on (11$\bar{2}$2) (96.4 ± 1.6)% of the (0001) growth rate. However, the In incorporation in figure 1(b) is very different. It is very low on the (11$\bar{2}$0) surface, only (30 ± 6)% of (0001) similar to reports in literature ([1] figure 12.2), while on the (11$\bar{2}$2) the In incorporation is (92 ± 2)% of a simultaneously grown (0001) sample.

This points to similar surface reconstructions on (11$\bar{2}$2) and (0001). On a closer look, the (11$\bar{2}$2) has an almost vertical nitrogen dangling bond, which is very similar to the (0001) surface [29]. Moreover, a metal ad-layer was observed too on (11$\bar{2}$2) GaN in molecular beam epitaxy [30] and was also a stable configuration in a calculations of the InGaN (11$\bar{2}$2) surface [29]. Hence, the (11$\bar{2}$2) show similar ad-layer reconstructions as (0001) and hence is also stable against

faceting, which is also confirmed by the straight interfaces observed by TEM and APT in figure 6 in section 3.3.

The activation energy for In desorption (fitted exponential lines in figure 1(b) was determined as (1.5 ± 0.4) eV for (11$\bar{2}$2) and (1.7 ± 0.3) eV for (0001) (see 1.9 eV for (0001) in [31]), which would further support comparable metal ad-layer reconstructions. Since steps usually enhance the desorption of surface species due to more dangling bonds, the slightly reduced In incorporation on (11$\bar{2}$2) may be caused by the tendency of the (11$\bar{2}$2) surface to form some additional atomic steps along [1$\bar{1}$00] and [$\bar{1}$100] which results in a long range undulation (see figure 5 or [32]), similar to GaAs (113) [33, 34] and Pt (110) [35].

The critical thickness for relaxation of (11$\bar{2}$2) InGaN on GaN is shown in figure 2 together with two calculations. The onset on full relaxation occurs on (11$\bar{2}$2) at similar thicknesses as on (0001), and it is approximated also by the same surface relaxation model (solid line in figure 2) as for (0001) [38].

The Fischer model used by Nishinaka *et al* in [36] (dashed line in figure 2) does not work well for full relaxation (0001) and hence (11$\bar{2}$2): it predicts relaxation too early for low In contents and too late for high In contents. Moreover, on (0001) the onset of relaxation is governed by the formation of dislocations above the interface, i.e a strained layer remains below a relaxed layer [38]. This is fundamental different from the dislocation movements in the Fischer and related models (see [38]).

However, in (11$\bar{2}$2) GaN one dimensional relaxation can proceed also by dislocation glide in the (0001) plane, which results in a tilt of the (0001) plane [36, 37, 39]. Thus, tilt and hence partial relaxation can set in slightly earlier on (11$\bar{2}$2) than full relaxation on (0001). Since the onset of tilt is connected with the glide of dislocations, the modified Fischer
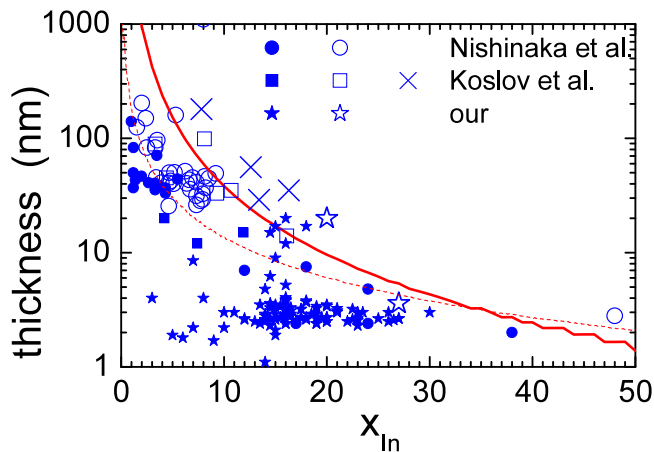
Figure 2. Strain state of several $(11\bar{2}2)$ InGaN QWs, which is either fully strained (solid symbols), tilted (open symbols), or fully relaxed ($\times$), obtained from our data $\star$ as well as from • [36], and ■ [37]. The solid line is a model for the critical thickness for InGaN on (0001) GaN from [38], and the dotted line is a modified Fischer model used by Nishinaka *et al* [36].

model of Nishinaka *et al* describes the onset of tilt (dashed line in figure 2).

Thus on $(11\bar{2}2)$ the dislocation glide results in tilt and partial relaxation. Dislocations occur along $[1\bar{1}00]$ only for larger thicknesses. The similarity of the critical thickness on (0001) and $(11\bar{2}2)$ suggest that new dislocation form on the growing surfaces above the interface when exceeding the critical thickness for full relaxation.

3.2. Optical properties

We systematically investigated the room temperature PL over the whole wavelength range. For (0001) and $(11\bar{2}2)$ QWs, the wavelength dependence of the integrated PL peak area in figure 3(a) shows the same trend as the reported internal quantum efficiency (IQE) on (0001) which remains constant between 410 and 480 nm [40]. A similar trend can be seen in the external quantum efficiency of (0001) LEDs [40–42]. However, compared to $(11\bar{2}2)$ the (0001) QWs on sapphire were always brighter by a factor of 4 up to 500nm as shown in figure 3(a), even though growth conditions were optimised for $(11\bar{2}2)$ QWs. The integrated PL intensity of $(11\bar{2}0)$ QWs in figure 3(a) was even less than a tenth of the (0001) QWs. Since the $(11\bar{2}2)$ and $(11\bar{2}0)$ LDD QWs were grown on patterned or freestanding GaN templates, these could have different light extraction efficiencies. Therefore, we compared QWs prepared directly on *m*- and *r*-plane sapphire (open symbols in figure 3(a)). The HDD templates further reduces the PL intensity by a factor of ≈ 2.5 compared to LDD templates [18]. Nevertheless the intensity ratio between $(11\bar{2}2)$ and $(11\bar{2}0)$ is similar for QWs on LDD and HDD templates between 400 and 440 nm. Hence light extraction cannot explain the reduced PL of the LDD semi- and non-polar QWs.

The $(11\bar{2}2)$ QWs on LDD templates have similar PL FWHMs as (0001) QWs up to 500 nm (figure 3(b)). Wernicke *et al* also found the smallest PL FWHMs for (0001), $(11\bar{2}2)$,
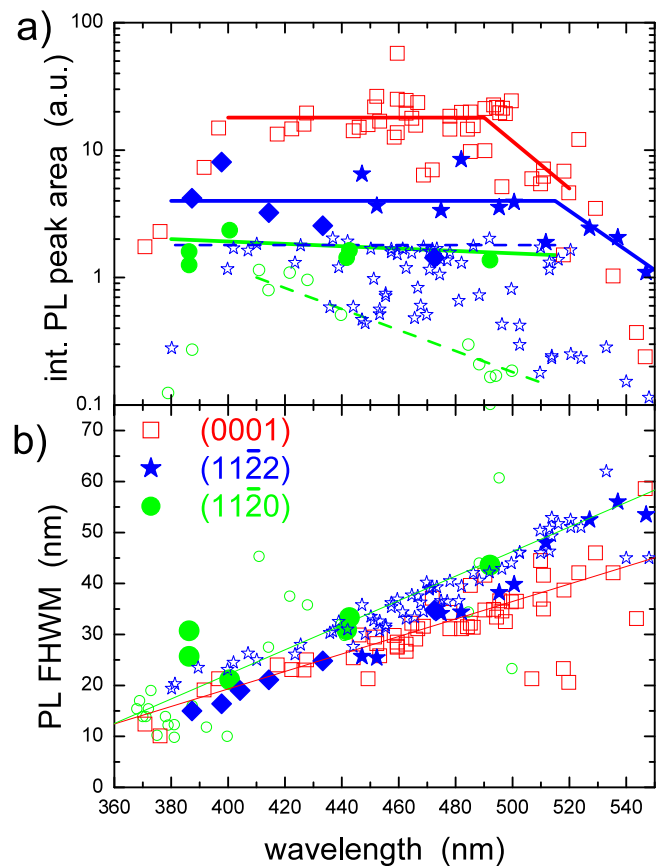

Figure 3. Room temperature PL integrated peak area (a) and FWHM (b) by excitation with a 0.25 mW 266 nm laser of 5× InGaN QWs on simultaneously grown (0001) (□), $(11\bar{2}2)$ (◆ ≈2 nm QWs, ★ 2.7–4 nm QWs) and $(11\bar{2}0)$ (•) using growth conditions optimised for $(11\bar{2}2)$. Solid symbols are on LDD templates, open ones are on unpatterned *c*-/*m*-/*r*-plane sapphire. The $(11\bar{2}2)$ and $(11\bar{2}0)$ QWs were between 2.5 and 4.0 nm thick, with typical barriers widths of 7 nm or 10 nm.

and $(1\bar{1}00)$ [9]. Our FWHMs are also consistent with the ones reported for $(11\bar{2}2)$ on freestanding GaN by Nishinaka *et al* [43].

The observed reduction in PL intensity in figure 3(a) is surprising given the higher wave function overlap in the semi- and non-polar QWs with reduced fields, which was demonstrated by much shorter PL lifetimes [44, 45]. But the observed lower PL intensities agree with lower reported IQE of semi-polar QWs, which barely exceed 50% for blue and drop for longer wavelengths [36, 43, 46]. In a direct comparison, the IQEs of bulk samples were less than 2/3 of QWs on (0001) GaN in the blue [47]. Only a single report found a higher IQE on *m*-plane bulk at 400 nm compared to *c*-plane on sapphire [48]. Indeed, high IQEs (or for LEDs external quantum efficiencies) up to 80% were reported on $(1\bar{1}00)$ near 400 nm [48–50]. But the IQEs quickly reduced towards longer wavelengths [51]. For comparison, on (0001) an IQE of 90% is routinely exceeded on *c*-plane sapphire between 410 and 480 nm e.g. [40]. It seems like the reduced fields are connected to reduced PL and IQE for blue and longer wavelengths.
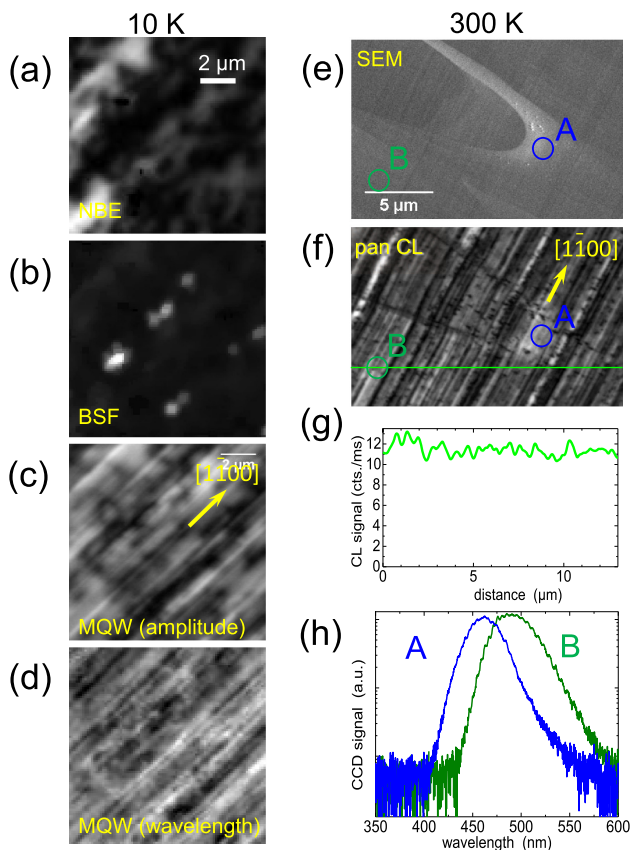
Figure 4. CL of a 5× MQW emitting near 490 nm. Left column at 10 K showing 11.2 × 11.2 μm^2. From top to bottom: (a) peak amplitudes at NBE (b) peak amplitude at BSF I$_1$ (c) amplitude in MQW (d) centre QW wavelength (black 488 nm to white 493 nm). The right column is on a larger scale from the same QWs at room temperature near a large surface feature. From top to bottom (e) SEM image (f) panchromatic amplitude (g) intensity along the marked line in (f) and (h) spectra at two positions near a slope with many steps (A) and on a flat region (B) as indicated in (e) and (f).

3.3. Microstructure

Due to the unexpected low PL intensity of samples on patterned substrate, we probed these QW by CL. Figures 4(a)–(c)
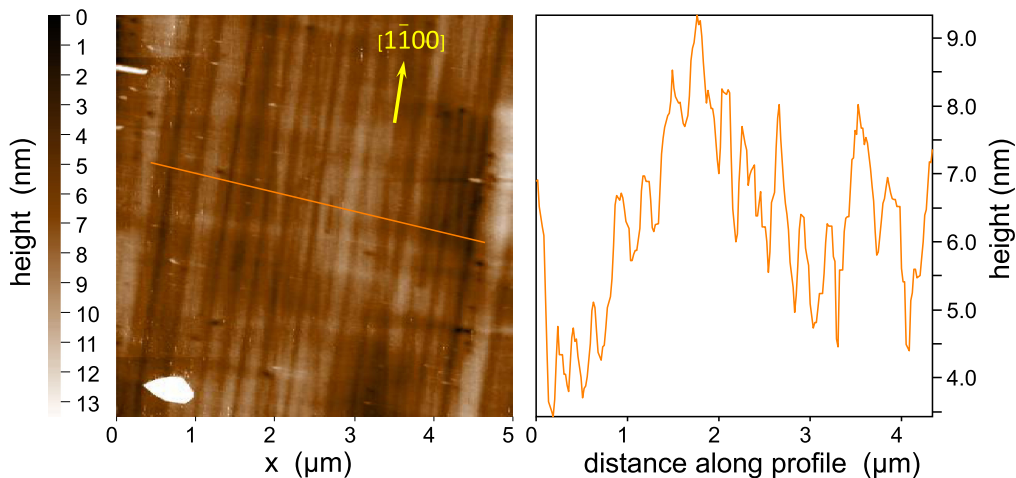
shows 10 K CL images of a QW structure emitting near 490 nm. Figure 4(a) shows the near band edge (NBE) CL which is enhanced in the former coalescence region of the patterns (compare to [8]), because the sidewalls and steps there tends to incorporate more residual oxygen. This leads to higher back doping and stronger NBE CL. The basal plane stacking faults (BSFs) light up only in few places (since the sample had a low density of 200–300 cm^{-1} BSFs). The BSFs are separated by multiples of 5 μm, indicating that the BSF are only present at the coalescence boundary of the patterns which had a 5 μm period [8]. The amplitude of the QW CL signal around 490 nm in figure 4(c) is dominated by narrow darker lines. These lines are narrower than the dark spots from threading dislocations or BSFs near the coalescence boundary. Moreover, the centre wavelength of the emission also reproduces the line pattern, with a tendency of shorter wavelengths to correlate with lower CL intensity (figure 4(d)).

At room temperature the secondary electron images (figure 4(e)) shows lines too. The corresponding panchromatic CL image (figure 4(f)) shows darker lines at the same positions, additional to the dark spots related to threading dislocations and broader dark regions in a 5 μm spacing related to BSF and other defects at the coalescence boundaries of the pattern. In a line profile in figure 4(g) the darker lines correspond to a variation of less than 10% of the total intensity. Moreover, in a region with many steps near the apex of a large feature the CL is shifted towards shorter wavelengths by more than 15 nm in figure 4(h). This suggests that the brightness modulation of the darker lines is due to a local variation of the indium content due to the surface step structure.

Plan view TEM did not reveal any defects that could be correlated with these darker lines, only BSFs separated by multiples of 5 μm. But AFM (figure 5) shows step-bunching, which has been reported before on (11$\bar{2}$2) GaN [32]. The spacing of the steps bunches is close to the spacing of the darker lines. Hence, while the height of step-bunching is small, the regions with more step edges have a more (11$\bar{2}$0) like bond arrangement and hence incorporate less In as discussed in section 3.1 and figure 1. Thus the step-bunching
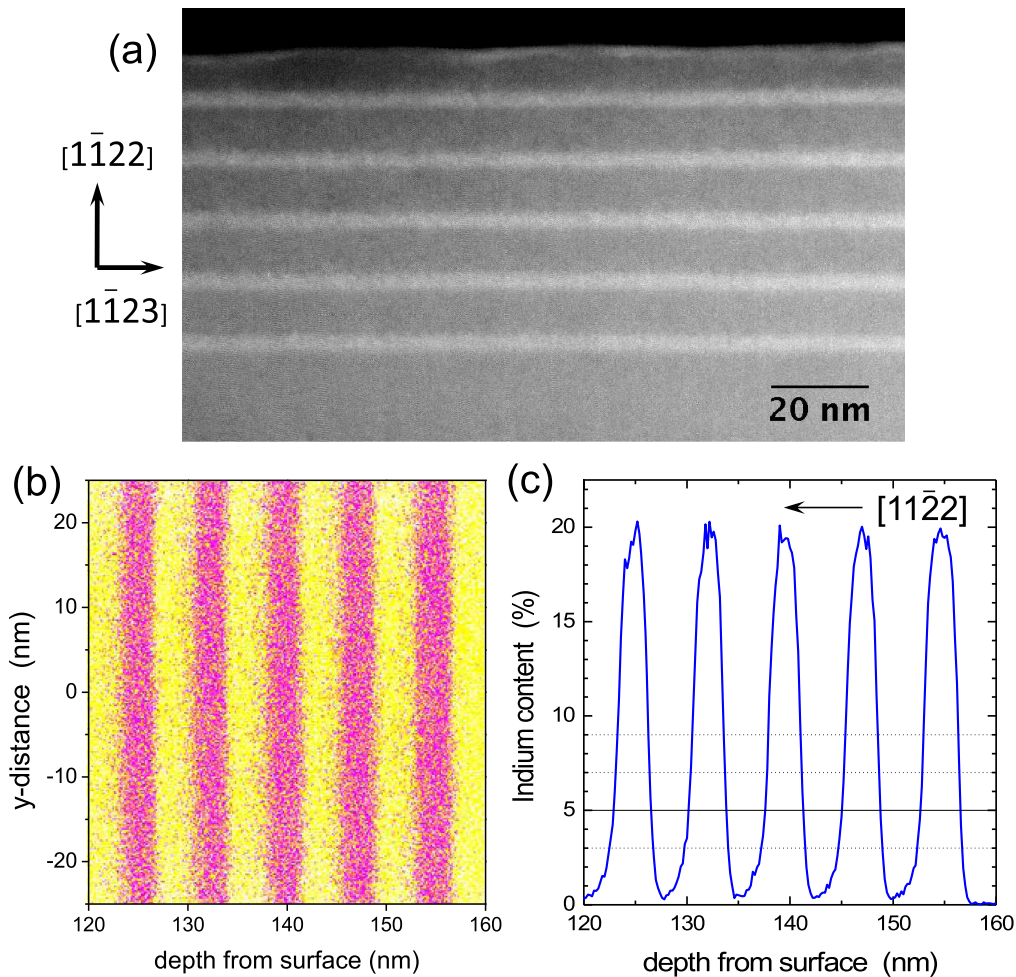

Figure 5. AFM image of a 5× QW emitting near 480 nm covered by 10 nm of GaN. The profile on the right shows step-bunching separated by 200–400 nm.

Figure 6. (a) TEM annular dark field along the [1$\bar{1}$00] zone axis of QWs in (11$\bar{2}$2) orientation on a patterned *r*-plane substrate. (b) The projection of an inner box of the atom positions obtained by APT shows well-defined QWs (Ga yellow, In purple), and the extracted In profile in (c) show only low In content in the barriers. The dotted line marks the different interface thresholds we used for the rms calculation, and the solid line the 5% criteria we chose for table 1.

causes a slight wavelength and intensity modulation of less than 10% (as seen in figure 4(g)).

This local variation could also explain the recent findings with scanning near field optical microscopy (SNOM) on (11$\bar{2}$2) QW, which found a narrowing of PL FWHM on (11$\bar{2}$2) QWs when reducing the SNOM aperture from 30 to 10 nm [52]. For the smaller aperture the sampling may have been limited to terraces, depending on the dimension of the step-bunching.

However, the total variation of emission intensity is less than 10% (see cross-section in figure 4(g)). This is well within the scattering of total PL intensities when reproducing a QW at the same wavelength on a different sample. Moreover, the density of dark spots (and correlated threading dislocations) is less than 10^8 cm^{-2}, i.e. lower than on the templates of the simultaneously grown (0001) QWs. Therefore, CL cannot explain the four times lower PL signal of (11$\bar{2}$2) QWs compared to (0001).

The TEM dark field image of a (11$\bar{2}$2) fivefold QW in figure 6(a) does not show much contrast variation over 120 nm. The QWs have a uniform thickness, and the interfaces appear sharp and straight without any dislocation in the

Table 1. Rms roughness from APT of the upper and lower interfaces (using a 5% In surface) of the first (deepest) to the last grown InGaN QW on (11$\bar{2}$2) with 20% In content. The analysed area was about 2400 nm^2, similar to that in [16].

QW No.	rms bottom (nm)	rms top (nm)
1st	0.26	0.27
2nd	0.29	0.54
3rd	0.31	0.36
4th	0.32	0.34
5th	0.30	0.41

field of view, especially compared to a 16% InGaN QW on (11$\bar{2}$0) [14]. The latter is expected, because of the low TDD density for regions away from the coalescence boundaries (see [8, 53]). The absence of QW undulation at this length scale supports our assumption that small changes in the local In content cause the small peak wavelength and intensity variation. Large area diffraction contrast images show that apart from the dislocations originating from the patterned
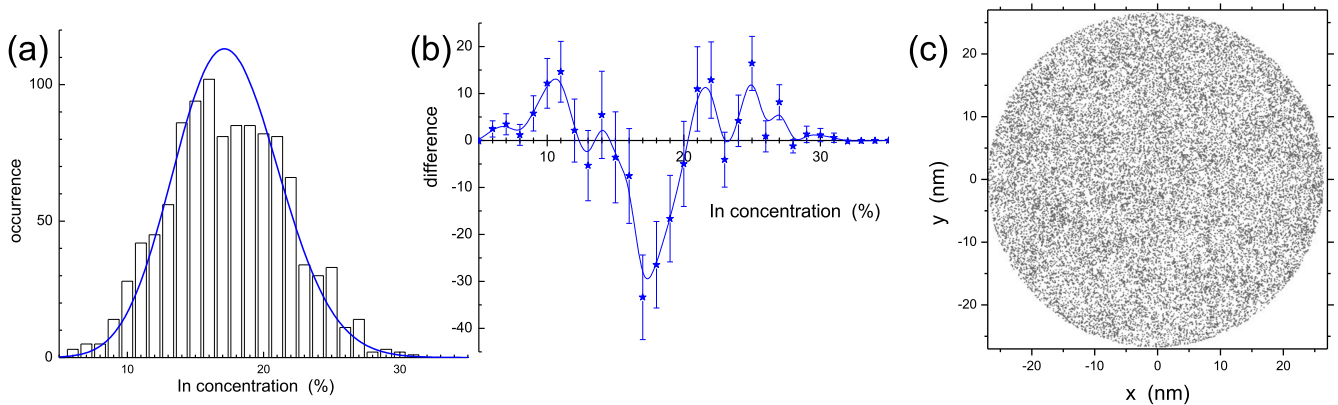
Figure 7. (a) Frequency distribution analysis with a bin size of 100 on the second QW shows a deviation from the random alloy hypothesis (line). The difference between the expected binominal distribution and the measured one is outside the error margins in (b). (The error bars are the square root of the measured values.) Despite this deviation the projected In positions in the second QW (c) show no obvious In-rich regions, unlike $(11\bar{2}0)$ [13].

GaN template, no new dislocations emerged from the QWs, i.e. the QWs were fully strained.

We performed APT of two $(11\bar{2}2)$ QWs and analysed them as described in [25]. We show here the data for the sample with the higher In content, which was 19%–20% In in XRD and APT (figure 6(c)). Thus all In contributes to strain (which is measured in XRD), which again confirms that the QWs are fully strained. Furthermore, the In content over depth in figure 6(c) shows low In segregation during growth compared to $(11\bar{2}0)$ [14] and thus a low In content in the GaN barriers and a sharp rise and fall of the In signal at the interfaces, in agreement to TEM.

To quantify the flat interfaces seen in figure 6, we determined the rms roughness for the lower and upper interface each of the five QWs from the APT data. We tried interfaces when the In concentration drops below 9%, 7%, 5%, or 3%. Below 5% the rms values of the upper and lower interfaces increased, since we reach the start of the In tails. Since at 5% the rms of the lower interface is still very close to the rms roughness for higher threshold levels, we choose 5% indium concentration as the interface criteria for table 1. With this criterion, the difference between the lower and upper interface was the largest. Even then, the lower and upper interfaces had nearly the same roughness as shown in table 1. Moreover, the rms roughness increased very little from the first to the last grown QW. For comparison on (0001), the rms roughness typically increases by a factor of two between the lower and upper QW interfaces even at lower In content [16]. This is due to some irregular island structure on (0001) InGaN which smoothens during GaN barrier growth [16, 54].

A frequency distribution analysis (FDA) of the In atoms was performed on the same APT data set on each of the five QWs. There is a statistically significant deviation from the random alloy hypothesis, i.e. the peak count in figures 7(a) and (b) is lower than expected for a random alloy. The magnitude of this deviation is more difficult to judge. The deviation on $(11\bar{2}2)$ seems less pronounced than the one observed of a 16% In containing $(11\bar{2}0)$ QW [13, 14],

although a direct comparison is not possible due to differences in sampling. Moreover, there are no obvious In-rich areas visible in the projected concentrations maps of $(11\bar{2}2)$ (figure 7(c)), which has been seen for $(11\bar{2}0)$ QWs [13]. In terms of non-random alloys the $(11\bar{2}2)$ surface is between the random alloy (0001) InGaN [15, 16] and the strongly nano-clustered $(11\bar{2}0)$ [13, 14], i.e. there seems a tendency to form In-rich areas which increases with increasing tilt towards $(11\bar{2}0)$.

From the FDA one would expect a stronger carrier localisation on $(11\bar{2}2)$ than on (0001) caused by the stronger variation of the local In content. This should lead to a broader PL FWHM at 300 K on $(11\bar{2}2)$. However, interface roughness as the other cause of localisation is reduced on $(11\bar{2}2)$ compared to (0001). The flat interfaces apparently compensate for the broadening due to In variation, and hence result in similar PL FWHM of $(11\bar{2}2)$ and (0001).

Overall, the flat interfaces and a small deviation from a random alloy were the only structural differences of $(11\bar{2}2)$ QWs to (0001) QWs.

4. Conclusion

In incorporation, growth rate, and the critical thickness of $(11\bar{2}2)$ QWs are slightly lower than (0001) QWs, while the In incorporation on $(11\bar{2}0)$ is reduced by a factor of three. Therefore, areas with more steps on $(11\bar{2}2)$ are more $(11\bar{2}0)$ like and incorporate slightly less In, resulting in shorter emission wavelength. A small step-bunching on $(11\bar{2}2)$ induces a small variation of the In content and emission intensity. The $(11\bar{2}2)$ QWs have very flat top interfaces compared to (0001), and a small tendency to form In-rich areas on the atomic scale. This does not lead to broader PL FWHMs, unlike $(11\bar{2}0)$. But compared to (0001), the observed PL intensities at 300 K were 1/4 for $(11\bar{2}2)$ QWs and even 1/10 for $(11\bar{2}0)$ QWs.

Acknowledgments

References

[1] Paskova T (ed) 2008 *Nitride Materials and Devices with Nonpolar Surfaces: Development and Prospects* (Weinheim, Germany: Wiley-VCH Verlag GmbH & Co. KGaA)

[2] Funato M, Kotani T, Kondou T, Kawakami Y, Narukawa Y and Mukai T 2006 *Appl. Phys. Lett.* **88** 261920

[3] Okada N, Kurisu A, Murakami K and Tadatomo K 2009 *Appl. Phys. Express* **2** 091001

[4] Leung B, Sun Q, Yerino C, Zhang Y, Han J, Kong B H, Cho H K, Liao K Y and Li Y L 2012 *J. Cryst. Growth* **341** 27–33

[5] Tendille F, Mierry P D, Vennégèus P, Chenot S and Teisseire M 2014 *J. Cryst. Growth* **404** 177–183

[6] Scholz F, Meisch T, Caliebe M, Schörner S, Thonke K, Kirste L, Bauer S, Lazarev S and Baumbach T 2014 *J. Cryst. Growth* **405** 97–101

[7] Okada N, Ishikawa A, Yamane K, Tadatomo K, Jahn U and Grahn H T 2014 *Phys. Status Solidi* a **211** 736–9

[8] Brunner F, Zeimer U, Edokama F, John W, Prasai D, Krüger O and Weyers M 2015 *Phys. Status Solidi* b **252** 1189–94

[9] Wernicke T, Schade L, Netzel C, Rass J, Hoffmann V, Ploch S, Knauer A, Weyers M, Schwarz U and Kneissl M 2012 *Semicond. Sci. Technol.* **27** 024014

[10] Wang Y, Shimma R, Yamamoto T, Hayashi H, Shiohama K, Kurihara K, Hasegawa R and Ohkawa K 2015 *J. Cryst. Growth* **416** 164–8

[11] Strittmatter A, Northrup J E, Johnson N M, Kisin M V, Spiberg P, El-Ghoroury H, Usikov A and Syrkin A 2011 *Phys. Status Solidi* b **248** 561–73

[12] Browne D A, Young E C, Lang J R, Hurni C A and Speck J S 2012 *J. Vac Sci. Technol.* A **30** 041513

[13] Tang F *et al* 2015 *Appl. Phys. Lett.* **106** 072104

[14] Griffiths J T *et al* 2016 *J. Appl. Phys.* **119** 175703

[15] Galtrey M J, Oliver R A, Kappers M J, Humphreys C J, Stokes D J, Clifton P H and Cerezo A 2007 *Appl. Phys. Lett.* **90** 061903

[16] Galtrey M J, Oliver R A, Kappers M J, Humphreys C J, Clifton P H, Larson D, Saxey D W and Cerezo A 2008 *J. Appl. Phys.* **104** 013524

[17] Prosa T J, Clifton P H, Zhong H, Tyagi A, Shivaraman R, DenBaars S P, Nakamura S and Speck J S 2011 *Appl. Phys. Lett.* **98** 191903

[18] Pristovsek M, Frentrup M, Han Y and Humphreys C J 2016 *Phys. Status Solidi* b **253** 61–6

[19] Kappers M J, Badcock T J, Hao R, Moram M A, Hammersley S, Dawson P and Humphreys C J 2012 *Phys. Status Solidi* c **9** 465–8

[20] Massabuau F C P *et al* 2014 *Appl. Phys. Lett.* **105** 112110

[21] Oliver R A *et al* 2013 *Appl. Phys. Lett.* **103** 141114

[22] Ju G, Honda Y, Tabuchi M, Takeda Y and Amano H 2014 *J. Appl. Phys.* **115** 094906

[23] Massabuau F C P, Davies M J, Blenkhorn W E, Hammersley S, Kappers M J, Humphreys C J, Dawson P and Oliver R A 2015 *Phys. Status Solidi* b **252** 928–35

[24] Sutherland D, Zhu T, Griffiths J T, Tang F, Dawson P, Kundys D, Oehler F, Kappers M J, Humphreys C J and Oliver R A 2015 *Phys. Status Solidi* b **252** 965–70

[25] Tang F, Moody M P, Martin T L, Bagot P A, Kappers M J and Oliver R A 2015 *Microsc. Microanal.* **21** 544–56

[26] Oehler F, Vickers M E, Kappers M J and Oliver R A 2013 *J. Appl. Phys.* **114** 053520

[27] Oehler F, Vickers M E, Kappers M J and Oliver R A 2013 *J. Appl. Phys.* **114** 219901 (Erratum)

[28] Ploch S, Wernicke T, Frentrup M, Pristovsek M, Weyers M and Kneissl M 2012 *Appl. Phys. Lett.* **101** 202102

[29] Northrup J E 2009 *Appl. Phys. Lett.* **95** 133107

[30] Lahourcade L, Renard J, Gayral B, Monroy E, Chauvat M P and Ruterana P 2008 *J. Appl. Phys.* **103** 093514

[31] Pristovsek M, Stellmach J, Leyer M and Kneissl M 2009 *Phys. Status Solidi* c **6** S565–9

[32] Ploch S, Wernicke T, Dinh D V, Pristovsek M and Kneissl M 2012 *J. Appl. Phys.* **111** 033526

[33] Nötzel R, Temmyo J and Tamamura T 1994 *Appl. Phys. Lett.* **64** 3557–9

[34] Pristovsek M, Menhal H, Wehnert T, Zettler J T, Schmidtling T, Esser N, Richter W, Setzer C, Platen J and Jacobi K 1998 *J. Cryst. Growth* **195** 1–5

[35] Hanesch P and Bertel E 1997 *Phys. Rev. Lett.* **79** 1523–6

[36] Nishinaka J, Funato M and Kawakami Y 2012 *J. Appl. Phys.* **112** 033513

[37] Koslow I L, Hardy M T, Hsu P S, Wu F, Romanov A E, Young E C, Nakamura S, DenBaars S P and Speck J S 2014 *J. Cryst. Growth* **388** 48 – 53

[38] Pristovsek M, Kadir A, Meissner C, Schwaner T, Leyer M, Stellmach J, Kruse A and Kneissl M 2013 *J. Cryst. Growth* **372** 65–72

[39] Kim J, Min D, Jang J, Lee K, Chae S and Nam O 2015 *Japan. J. Appl. Phys.* **54** 02BA02

[40] Chichibu S, Sota T, Wada K, Brandt O, Ploog K, DenBaars S and Nakamura S 2001 *Phys. Status Solidi* a **183** 91–8

[41] Jun-Lin L *et al* 2015 *Chin. Phys.* B **24** 067804

[42] Pristovsek M, Humphreys C J, Bauer S, Knab M, Thonke K, Kozlowski G, O'Mahony D, Maaskant P and Corbett B 2016 *Japan. J. Appl. Phys.* **55** 05FJ10

[43] Nishinaka J, Funato M and Kawakami Y 2015 *Appl. Phys. Lett.* **106** 082105

[44] Ueda M, Kojima K, Funato M, Kawakami Y, Narukawa Y and Mukai T 2006 *Appl. Phys. Lett.* **89** 211907

[45] Funato M and Kawakami Y 2008 *J. Appl. Phys.* **103** 093501

[46] Wang J, Meisch T, Heinz D, Zeller R and Scholz F 2016 *Phys. Status Solidi* b **253** 174–9

[47] Jönen H *et al* 2011 *Appl. Phys. Lett.* **99** 011901

[48] Lee J, Li X, Ni X, Özgür U, Morkoç H, Paskova T, Mulholland G and Evans K R 2009 *Appl. Phys. Lett.* **95** 201113

[49] Garrett G A, Shen H, Wraback M, Tyagi A, Schmidt M C, Speck J S, DenBaars S P and Nakamaura S 2009 *Phys. Status Solidi* c **6** S800–3

[50] Yokogawa T and Inoue A 2014 *Proc. SPIE* **9003** 900316

[51] Lin Y D, Chakraborty A, Brinkley S, Kuo H C, Melo T, Fujito K, Speck J S, DenBaars S P and Nakamura S 2009 *Appl. Phys. Lett.* **94** 261108

[52] Funato M and Kawakami Y 2015 *Proc. SPIE* **9363** 93631T

[53] Han Y, Caliebe M, Hage F, Ramasse Q, Pristovsek M, Zhu T, Scholz F and Humphreys C 2016 *Phys. Status Solidi* b **253** 834–9

[54] Pristovsek M, Kadir A, Meissner C, Schwaner T, Leyer M and Kneissl M 2011 *J. Appl. Phys.* **110** 073527